Molecular Cancer Therapeutics

# Photodynamic Therapy Using Indocyanine Green Loaded on Super Carbonate Apatite as Minimally Invasive Cancer Treatment

Koki Tamai[1], Tsunekazu Mizushima[1], Xin Wu[2], Akira Inoue[1], Minori Ota[2], Yuhki Yokoyama[2], Norikatsu Miyoshi[1], Naotsugu Haraguchi[1], Hidekazu Takahashi[1], Junichi Nishimura[1], Taishi Hata[1], Chu Matsuda[1], Yuichiro Doki[1], Masaki Mori[1], and Hirofumi Yamamoto[1,2]

## Abstract

Minimally invasive treatment is getting more and more important in an aging society. The purpose of this study was to explore the possibility of ICG loaded on super carbonate apatite (sCA) nanoparticles as a novel photodynamic therapy (PDT) against cancers. Using colon cancer cells, ICG uptake and anti-tumor effects were examined between the treatments of ICG and sCA-ICG. Reactive oxygen species (ROS) production and temperature rise were also evaluated to explore the underlying mechanism. Atomic force microscopy revealed that the size of sCA-ICG ranged from 10 to 20 nm. In aqueous solution with 0.5% albumin, the temperature increase after laser irradiation was 27.1°C and 23.1°C in sCA-ICG and ICG, respectively (control DW: 5.7°C). A significant increase in ROS generation was noted in cell cultures treated with sCA-ICG plus irradiation compared with those treated with ICG plus irradiation ($P < 0.01$). Uptake of ICG in the tumor cells significantly increased in sCA-ICG compared with ICG *in vitro* and *in vivo*. The fluorescence signals of ICG in the tumor, liver, and kidney faded away in both treatments by 24 hours. Finally, the HT29 tumors treated with sCA-ICG followed by irradiation exhibited drastic tumor growth retardation ($P < 0.01$), whereas irradiation of tumors after injection of ICG did not inhibit tumor growth. This study shows that sCA is a useful vehicle for ICG-based PDT. Quick withdrawal of ICG from normal organs is unique to sCA-ICG and contrasts with the other nanoparticles remaining in normal organs for a long time. *Mol Cancer Ther; 17(7); 1613–22. ©2018 AACR.*



## Introduction

Photodynamic therapy (PDT) is a minimally invasive cancer treatment. The anti-tumor effect is thought to be caused by reactive oxygen species (ROS) and fever through excitation of photosensitizers (1–2). The U.S. Food and Drug Administration (FDA) and European Medicines Agency have approved photosensitizers temoporfin and methyl-aminolaevulic acid (MAL) for the treatment of head and neck cancer and skin cancer, and porfilimer sodium for esophageal and lung cancer (3). Because of its local action, PDT is expected to be minimally invasive and produce fewer adverse events than current cancer treatments, such as surgical resection, chemotherapy, and radiotherapy (4). Accordingly, PDT is considered to be a suitable therapy for elderly patients and high-risk patients who cannot endure the conventional treatments (5–6).

Several photosensitizers are currently in clinical use for limited species of diseases, mainly superficial cancers because their excitation light (630–670 nm) has low tissue permeability and reaches only the lesion at a depth of 0.8 to 1.2 mm (7–9). Another problem is that patients are obligated to stay in a dark room for 1 to 4 weeks after PDT to avoid light hypersensitivity. This long shielding time largely restricts patients' activities and makes clinical application of PDT somewhat difficult. To increase the indication and usability of PDT, further development of photosensitizers is needed (10–12).

Indocyanine green (ICG) is an FDA-approved water-soluble anionic tricarbocyanine dye. As ICG has low toxicity, it is used for various medical examinations, such as the measurement of cardiac output and hepatic function, ophthalmic angiography, and the detection of sentinel lymph nodes (13–16). In addition, ICG has the properties to act as a near-infrared ray (NIR) photosensitizer for PDT, generating heat and ROS by NIR irradiation (17). Because of its short half-life of 3 minutes, light shielding is not necessary after treatment. The relatively long wavelength of NIR has an advantage of reaching 4 to 6 times deeper lesion, compared with current photosensitizers (7–8). However, there are intrinsic drawbacks to systemic administration of ICG for PDT, including concentration-dependent aggregation, quick degradation, and low tumor specificity (18–20). To enhance the stability and tumor accumulation of ICG, certain nanocarriers are necessary. Various nanoplatforms, including liposome, polymeric micelles, and other specifically designed nanoparticles, have enabled effective delivery of ICG

[1]Department of Gastroenterological Surgery, Graduate School of Medicine, Osaka University, Suita city, Osaka, Japan. [2]Division of Health Sciences, Department of Molecular Pathology, Graduate School of Medicine, Osaka University, Suita City, Osaka, Japan.

**Note:** Supplementary data for this article are available at Molecular Cancer Therapeutics Online (http://mct.aacrjournals.org/).

**Corresponding Author:** Hirofumi Yamamoto, Osaka University, Yamadaoka1-7, Suita City, Osaka, 565-0871, Japan. Phone/fax: 81-6-6879-2591; E-mail: hyamamoto@sahs.med.osaka-u.ac.jp

**doi:** 10.1158/1535-7163.MCT-17-0788

to the tumor site (21–26). The nanoparticles are expected to accumulate in tumor tissues based on the enhanced permeability and retention (EPR) effect, which is explained by increased leakage via poorly aligned vascular endothelial cells and impaired lymphatic drainage (18, 27). On the other hand, there is a concern that nanoplatforms incorporating ICG retain large amounts in normal organs due to the prolonged biostability of ICG. Although ICG is thought to be a harmless reagent, the safety of long-term exposure in a single organ is unclear.

The carbonate apatite consisting of biocompatible inorganic ions ($CO_3^{2-}$, $Ca^{2+}$, and $PO_4^{3-}$) is a superior vehicle carrying siRNA into tumor cells (28). A super carbonate apatite (sCA) is a nanoparticle for *in vivo* delivery and the advantages of sCA are easy production, safe constituents, and rapid uptake by the tumor (29). We previously reported the *in vivo* safety and potent anti-tumor effects of sCA for delivery of doxorubicin, microRNAs, and siRNAs (29–34). In the present study, we evaluated the utility of ICG loaded on sCA (sCA-ICG) for delivery to the tumor and retention of ICG in normal organs. Using a NIR wavelength of 808 nm, we also examined anti-tumor effects to explore the possibility of sCA-ICG as a novel PDT.

## Materials and Methods

### Cell lines and cell culture

Human CRC cell lines HT29 and HCT116 were obtained from the ATCC in 2001. Stocks were prepared after passage 2 and stored in liquid nitrogen. All experiments were performed with cells of passage of <8. These cell lines were authenticated by morphologic inspection, short tandem repeat profiling, and Mycoplasma testing by the ATCC. *Mycoplasma* testing was also done by the authors in 2015. Cells were cultured in the DMEM containing 10% FBS at 37°C in a humidified incubator with 5% $CO_2$

### Formulation of sCA-ICG

$CaCl_2$ (4 μL, 1 mol/L) was mixed in 1 mL of inorganic solution (44 mmol/L $NaHCO_3$, 0.9 mmol/L $NaH_2PO_4$, 1.8 mmol/L $CaCl_2$, pH 7.5) with 40 μg ICG, followed by incubation at 37°C for 30 minutes. The solution was centrifuged at 17,000 × *g* for 3 minutes and the pellet dissolved in medium for *in vitro* use or distilled water containing 0.5% albumin for *in vivo* injection. The products in the solution were sonicated (38 kHz, 80 W) in a water bath before *in vitro* or *in vivo* use. The particle size was measured by atomic force microscopy using a SPM-9500 scanning probe microscope (Shimazu, Kyoto, Japan). Atomic force microscopy images were obtained by an AFM 5300E (Hitachi High-Technologies Co., Tokyo, Japan). After treatment of 0.01 mol/L EDTA, ICG amount incorporated in sCA was calculated with the calibration curve, and encapsulation efficiency was determined.

### Detection of reactive oxygen species

Aminophenyl fluorescein (APF; Goryo Chemical) was used to measure reactive oxygen species (ROS) generation. APF fluorescence were visualized by fluorescence microscopy with excitation at 470 nm and emission at 520 nm. The extent of APF fluorescence was quantified by a microplate reader (SH-900Lab, Hitachi High-Tech Science Co., Tokyo, Japan) or by the BD FACSCATO II flow cytometer.

### *In vitro* cellular uptake of ICG

To assess extent of ICG uptake, the cells were observed by fluorescence microscopy (BZ-X710, Keyence) with excitation at 750 to 800 nm and emission at 817.5 to 872.5 nm. Cellular uptake of ICG was analyzed quantitatively by the BD FACSCATO II flow cytometer.

### *In vitro* photodynamic therapy

A total of $1 \times 10^4$ cells were seeded onto 96-well cell culture plates. The next day, the cells were incubated with sCA alone, free ICG or sCA-ICG for 3 hours. The ICG concentration for HCT116 and HT29 cells was 20 and 10 μg/mL, respectively. The plate was then placed in the digital water bath to maintain the temperature at 37°C. The cells were then irradiated with an 808-nm laser with an energy density of 1 W/cm$^2$ for 1, 3, or 5 minutes. Twenty-four hours later, cell viability was quantified by MTT assay.

### Tumor xenograft mouse model

Five-week-old female BALB/cAJcl-nu/nu mice were purchased from CLEA Japan. The mice were housed in autoclaved cages and maintained under a 12 hours light/dark cycle with free access to food and water. To establish the tumor model, HT29 cells ($3 \times 10^6$ in a 100 μL Matrigel/DMEM) were administered subcutaneously. The tumor size was measured using digital vernier calipers and tumor volumes calculated as (width$^2$ × length)/2, where width and length correspond to the minor and major axes of the tumors. All experiments using mice were approved by the Institutional Animal Care and Use Committee Osaka University Graduate School of Medicine and the Committee for the Ethics of Animal Experiments of Osaka University (Approval numbers: 24-122-001 and 23-023-001).

### *In vivo* tumor imaging

When the tumor volume reached 300 to 400 mm$^3$, either free ICG or sCA-ICG was injected via the tail vein at an ICG dose of 5 mg/kg (100 μg of ICG in 200 μL injection). Whole-body imaging and *ex vivo* tumor imaging were performed using the IVIS Spectrum CT instrument (Perkin Elmer) at 2,4, 8, and 24 hours post-injection. The fluorescence intensity of organs, including the heart, lungs, kidney, liver, and spleen, was also quantified 4 and 24 hours post-injection.

### *In vivo* photodynamic efficiency and toxicity in major organs

At a tumor volume of 200 to 300 mm$^3$, the mice were randomized into three treatment groups ($n = 7$ in each group) and administered 200 μL of PBS, free ICG, or sCA-ICG (100 μg of ICG per mouse). The tumor regions of mice receiving free ICG or sCA-ICG were irradiated with an 808-nm laser for 5 minutes at a power density of 3.7 W/cm$^2$ 4 hours post-injection. Uniform irradiation of the treatment area was achieved using a rotating irradiation system. The tumor size and body weight were recorded every 2 days.

## Results

### Formulation of sCA-ICG

The sCA nanoparticles consisting of inorganic ions (i.e., $CO_3^{2-}$, $Ca^{2+}$, and $PO_4^{3-}$) were reduced to nanosize by sonication (Fig. 1A). Atomic force microscopy revealed that the size of sCA-ICG ranged from 10 to 20 nm (Fig. 1B). The

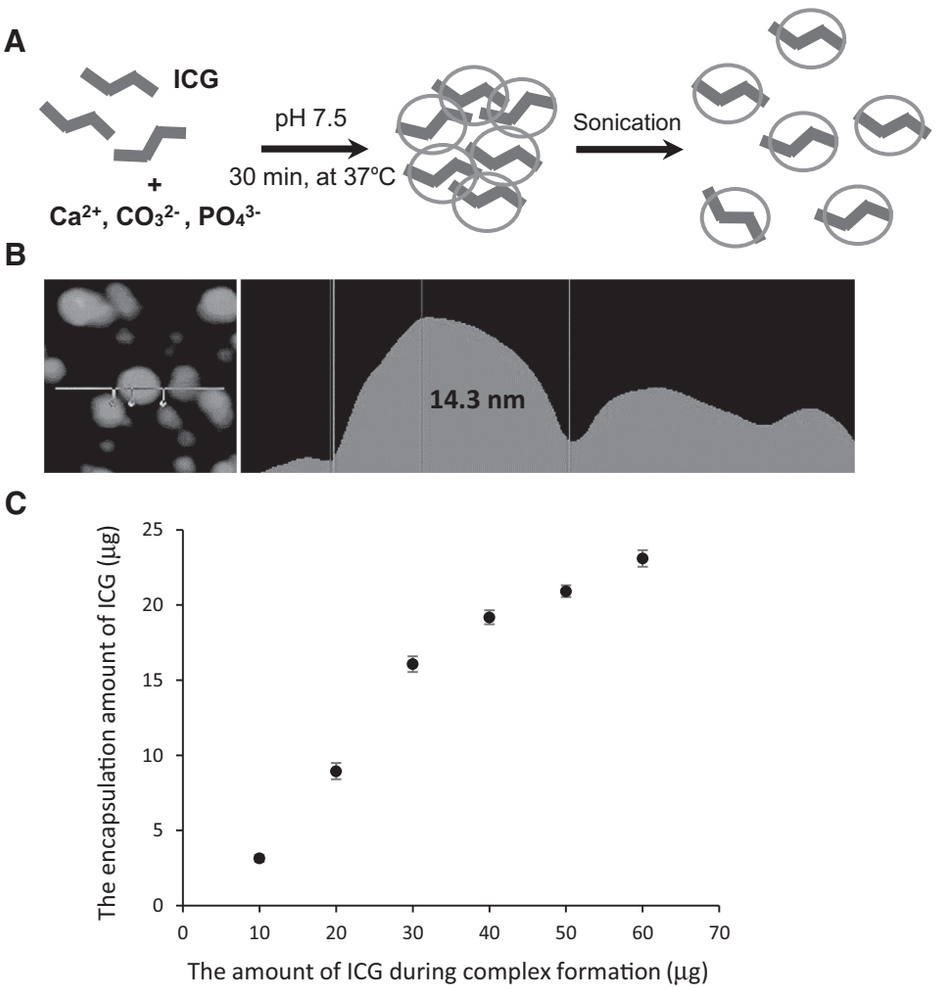


**Figure 1.**
Characteristics of sCA-ICG particles. **A,** Schematic of the generation of sCA incorporating ICG. **B,** AFM analysis for visualization of the nanoparticles. The sCA-ICG particle was approximately 15 nm. **C,** Encapsulation amount of ICG and the amount of ICG added during complex formation. After treatment of 0.01 mol/L EDTA, ICG amount incorporated in sCA was calculated with the calibration curve, and encapsulation efficiency was determined.

encapsulation amount of ICG loaded in sCA was 19.2 μg when 40 μg of ICG was added during complex formation, which is a binding affinity of 48.0% (Fig. 1C).

### Characterization of sCA-ICG

We investigated the characteristics of sCA-ICG in aqueous solution (i.e., absorbance, temperature increase, and ROS generation) compared with free ICG. As shown in Fig. 2A, free ICG had a clear monomer absorbance peak at 779 nm and a dimer peak at 720 nm. sCA-ICG solution also had two peaks at 779 nm and 720 nm. In the presence of 0.5% albumin, the absorption peaks shifted to the higher range, 803 nm, where NIR can excite. Under these conditions, the monomer peak of sCA-ICG became clear and the peak absorbance of sCA-ICG was 1.4-times higher than that of ICG (Fig. 2B). To examine the photothermal efficiency of ICG and sCA-ICG, we examined the temperature increase after laser irradiation for 6 minutes. In aqueous solution, the temperature increase for ICG and sCA-ICG was 17.6°C and 16.8°C, respectively, whereas distilled water was only 4.0°C (Fig. 2C). On the other hand, the temperature increase for ICG plus 0.5% albumin and sCA-ICG plus 0.5% albumin was 23.1°C and 27.1°C, respectively, whereas the temperature rise of distilled water was only 5.7°C. After irradiation for 5 minutes, sCA-ICG produced ROS to some extent, whereas only negligible ROS were generated in free ICG solution. In the presence of 0.5% albumin, the fluorescence intensity of ROS increased in both solutions. sCA-ICG produced a significantly higher level of ROS than free ICG ($P < 0.01$, Fig. 2D).

### *In vitro* cellular uptake

Fluorescence microscopy revealed a higher red fluorescence intensity at 3 hours in sCA-ICG–treated HCT116 and HT29 cells than cells treated with free ICG (Fig. 3A–D). Flow cytometry confirmed that both cell lines had a higher fluorescence intensity 3 and 6 hours after treatment with sCA-ICG than treatment with ICG alone ($P < 0.01$, Fig. 3E and F).

### *In vitro* cell viability

Without laser irradiation, the cell viability of HCT116 cells incubated with sCA-ICG at various concentrations for 24 or 48 hours was almost equivalent to that of cells treated with free ICG, indicating that sCA itself is not toxic (Supplementary Fig. S1). We then evaluated the *in vitro* photothermal antitumor effects. Irradiation was performed for 1, 3, and 5 minutes after 3 hours incubation of HCT116 or HT29 cells with sCA-ICG, ICG solution (20 μg/mL ICG for HCT116 and 10 μg/mL ICG for HT29), or sCA alone, followed by MTT assay 24 hours post-irradiation (Fig. 4A). Treatment with sCA plus

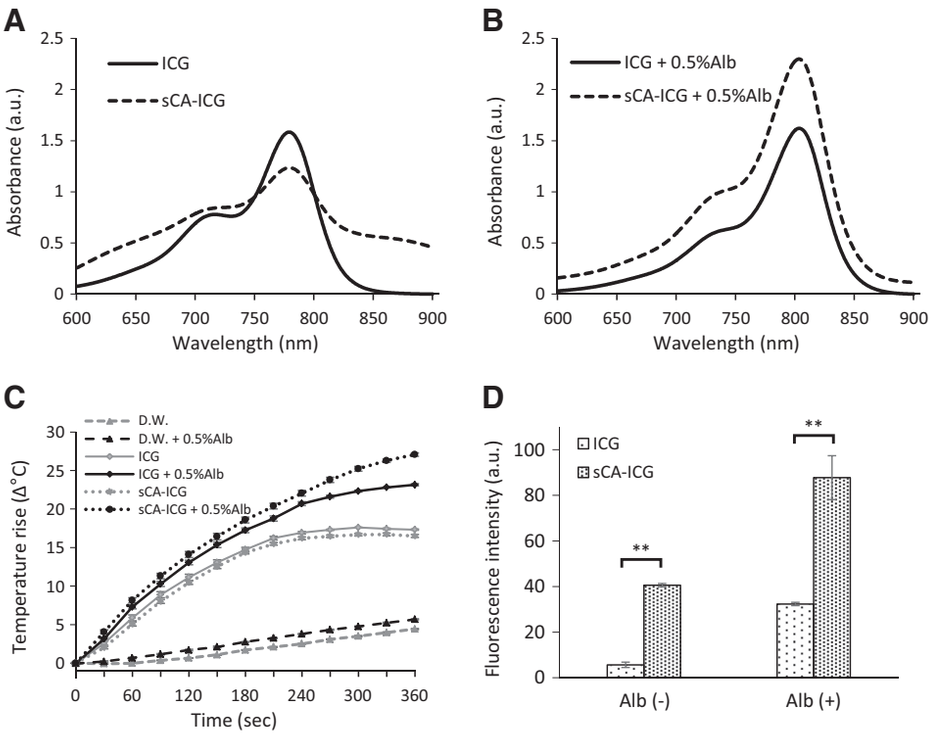


**Figure 2.**
Features of sCA-ICG and free ICG in aqueous solution. **A,** Absorption spectra. **B,** Absorption spectra with the addition of 0.5% albumin. The absorption spectra were recorded on a U-2900 UV/vis spectrometer (Hitachi High-Technologies Co.). **C,** Temperature increase after laser irradiation. Free ICG or sCA-ICG solution (20 μg/mL ICG) in a 96-well plate was irradiated using a DVL-20 (ASUKAMEDICAL CO., LTD, Osaka, Japan) with an 808-nm laser at 1 W/cm$^2$ for 6 min. No cells were present here. The temperature was measured by thermography. **D,** Intensity of the ROS signal after free ICG or sCA-ICG solution (20 μg/mL ICG) containing 2.5 μmol/L of APF was irradiated by the 808-nm laser at 1 W/cm$^2$ for 5 min. No cells were present here; **, $P < 0.01$.

irradiation showed no significant difference in cell viability when compared with no treatment with irradiation in both cell lines at all time points. In both cell lines, sCA-ICG plus irradiation resulted in significantly lower cell viability than free ICG plus irradiation or sCA plus irradiation at 5 minutes ($P < 0.01$, Fig. 4B and C).

Without irradiation, ROS generation was not observed by fluorescence microscopy (Fig. 4D and E), and only background signals were recorded by FACS (Fig. 4F–G). On the other hand, the clear green fluorescence of cellular ROS was evidently observed after treatment with sCA-ICG plus 5 minutes of irradiation (Fig. 4D and E). A significant increase in the mean fluorescence intensity of ROS generation was noted by FACS in cell cultures treated with sCA-ICG plus irradiation compared with those treated with free ICG plus irradiation ($P < 0.01$; Fig. 4F and G).

### *In vivo* and *ex vivo* fluorescence imaging and biodistribution

Next, we assessed the tumor accumulation and biodistribution in the mouse body after sCA-ICG treatment compared with free ICG. Before injection, no fluorescence signal was visible on the body surface of mice. At 4 and 8 hours, only weak fluorescence signals were detectable at the tumor and abdomen in ICG-injected mice, whereas strong fluorescence signals remained at the tumor, abdomen, and liver in sCA-ICG–injected mice. Fluorescence signals disappeared at 24 hours in both ICG- and sCA-ICG-injected mice (Fig. 5A).

*Ex vivo* experiments revealed that the ICG fluorescence was much more evident in the sCA-ICG group than the ICG group at the tumor and liver 4 hours after injection (Fig. 5B). The fluorescence intensity in the tumor decreased in a time-dependent manner and was 1.6, 2.0, and 1.5-times higher in the sCA-ICG group than that the ICG group at 2, 4, and 8 h, respectively ($P < 0.05$, Fig. 5C). In the normal organs, considerable fluorescence signals were noted in the liver and kidney in the sCA-ICG group, whereas the signal was weak in the heart, lung, and spleen at 4 hours (Fig. 5D). A significant increase in the fluorescence signal was observed in the tumor and liver in the sCA-ICG group compared with the ICG treatment group at 4 and 8 hours (*, $P < 0.05$ and **, $P < 0.01$). The fluorescence signals mostly faded away in both groups by 24 hours (Fig. 5D).

### *In vivo* anti-tumor effects of NIR laser irradiation on tumors treated with sCA-ICG

Finally, we examined the *in vivo* antitumor effects of NIR laser irradiation on HT29 tumors. Irradiation of tumors after injection of ICG did not result in significant tumor growth retardation. In contrast, the tumors treated with sCA-ICG followed by irradiation exhibited drastic and significant tumor growth retardation compared to those treated with laser irradiation after ICG injection ($P < 0.01$, Fig. 6A and B). No obvious body weight loss was observed in either treatment group (Fig. 6C). In addition, we confirmed that repeat administration of sCA-ICG (6 times injections in 14 days) did not cause hepatotoxicity or other severe adverse events in mice (Supplementary Fig. S2).

## Discussion

ICG is expected to be a biologically safe photosensitizer. However, due to rapid metabolism and a low tumor specificity of ICG, it is difficult to use ICG alone for PDT. Therefore, various carriers have been developed to deliver ICG to tumors; however, these carriers keep ICG in normal organs for a longer duration (21–23, 35–37). The present study demonstrated for the first time that sCA incorporating ICG efficiently

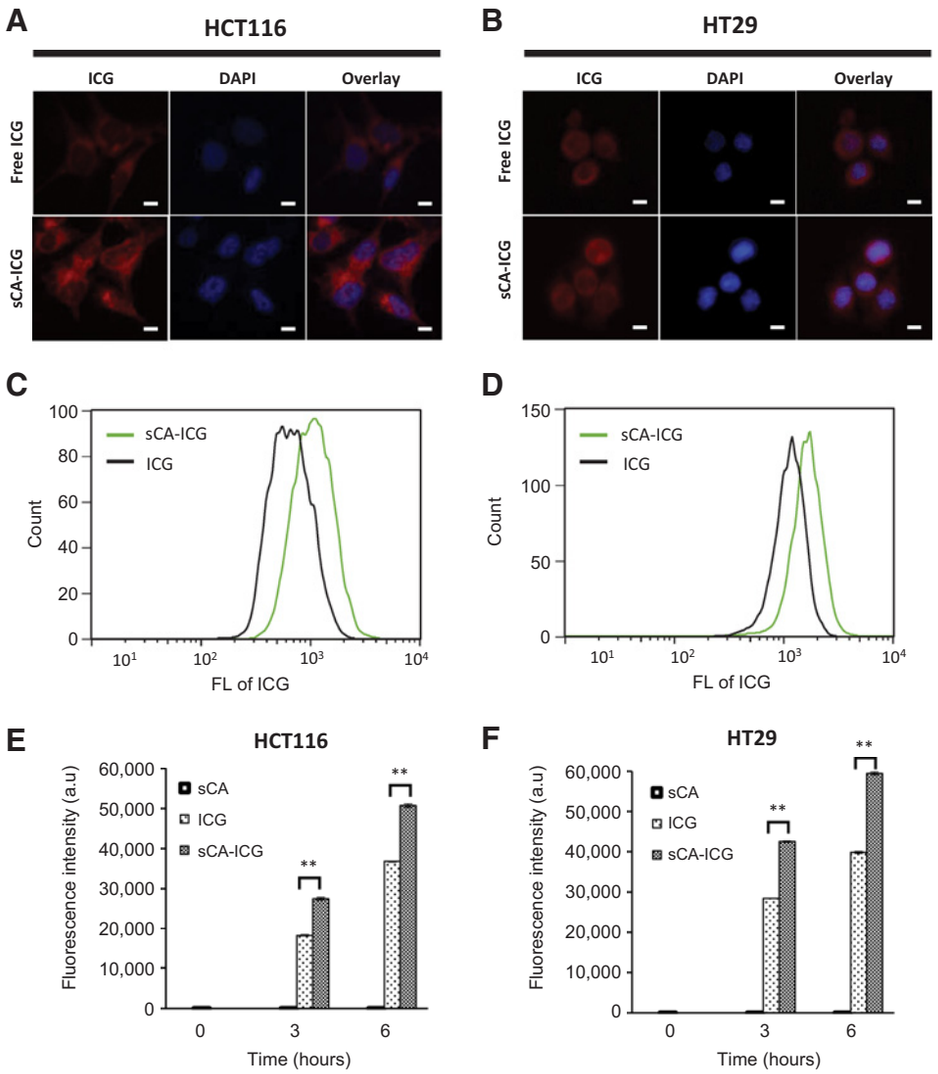


**Figure 3.**

*In vitro* cellular uptake of ICG and sCA-ICG. **A** and **B,** Fluorescence images of HCT116 and HT29 cells after 3 hours of incubation with free ICG and sCA-ICG. A total of $4 \times 10^5$ cells were seeded onto 6-well plates. The medium was exchanged for medium containing 20 μg/mL free ICG or sCA-ICG containing the same concentration of ICG. At 3 and 6 hours, the cells were fixed with 4% paraformaldehyde solution for 20 minutes and nuclei stained with 4,6-diamidino-2-phenylindole (DAPI) solution. The cells were observed by fluorescence microscopy with excitation at 750–800 nm and emission at 817.5–872.5 nm; scale bar, 5 μm. **C** and **D,** Flow cytometric analysis of HCT116 and HT29 cells after 3 hours incubation with free ICG and sCA-ICG. A total of $5 \times 10^5$ cells were seeded on 6-well plates. Attached cells were grown in cultures containing 20 μg/mL free ICG or sCA-ICG (containing 20 μg/mL ICG) for 3 hours. The fluorescence histograms of ICG were measured with a flow cytometer. **E** and **F,** Quantitative comparison of fluorescence intensity in HCT116 and HT29 cells at 3 and 6 hours. Flow cytometry showed that both cell lines had a higher fluorescence intensity 3 and 6 hours after treatment with sCA-ICG than treatment with ICG alone; **, $P < 0.01$.

accumulated in tumors, exhibiting potent antitumor effects with NIR laser irradiation, without remaining in normal organs for a long time.

sCA achieved innovative delivery of nucleic acids to various tumors for *in vivo* use. With this system, we previously reported that the nucleic acid medicine accumulated in tumor cells within 2 to 4 hours after injection via the tail vein. Because of its sensitivity to acidic environments, siRNA can easily escape from endosomes to the cytoplasm (29, 30). In this study, we made sCA particles incorporating ICG via a quite simple procedure (Fig. 1A). A 20-nm gold colloid particle has been demonstrated to permeate into the deep lesion of tumors far from vessel centers, but 100-nm particles remain around vessels (38). Carbal and colleagues also reported that nanomedicines smaller than 50 nm can penetrate into poorly permeable hypovascular tumors, whereas sub–100-nm micellar nanomedicines exhibit limited permeation (39). Therefore, sCA-ICG < 20 nm may have an advantage in penetrating deep into the tumor, regardless of the tumor vasculature. Approximately 50% of the ICG was incorporated into sCA (Fig. 1C). As doxorubicin has reportedly been shown to be incorporated at less than 1% in carbonate apatite (30), the 50% binding affinity of sCA for ICG would be acceptable considering the economical cost of ICG.

Free ICG binds to serum albumin and lipoproteins and constitutes high molecular compound in the blood stream. We also use 0.5% albumin for coating sCA to maintain the nanoparticle dispersal (29). Carbonate apatite particles are likely to bind to albumin because the zeta potential shifts to further negative when mixed with albumin (40). Moreover, it is reported that coating of liposomal ICG nanoparticles with albumin remarkably improved stability (41). To analyze the appropriate wavelength for absorption in both ICG and sCA-ICG solution, we added 0.5% albumin; the monomer absorbance peak shifted to the higher wavelength at 803 nm where NIR excites. This change was advantageous because NIR can penetrate the tumor much deeper than conventional laser beams (42). NIR irradiation led to a large increase in temperature, possibly because the light absorption was efficiently converted to heat. ROS production could be one reason for the superior anti-tumor effects of sCA-ICG over free ICG. For sCA-ICG, ROS production was further enhanced in the presence

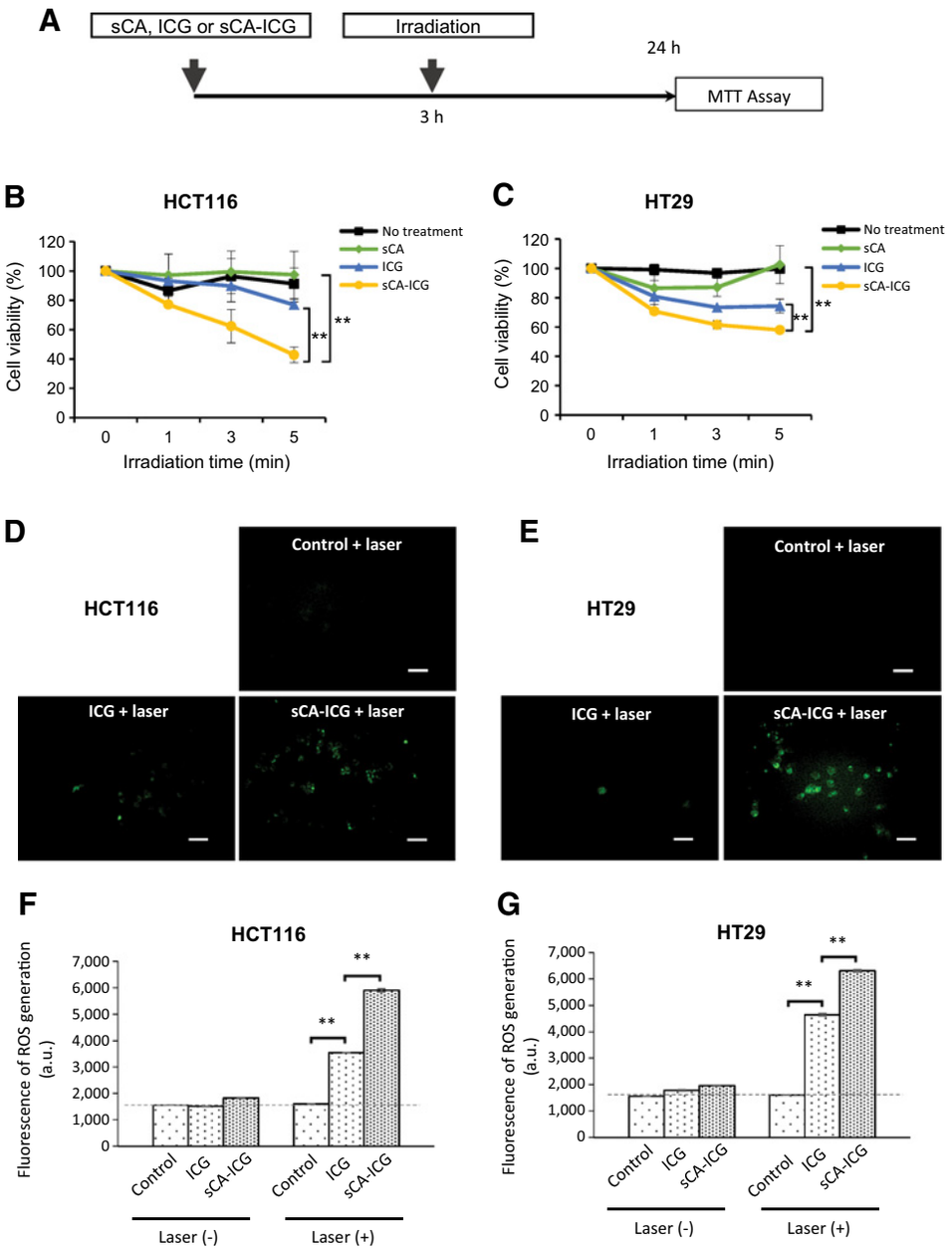


**Figure 4.**

*In vitro* cell viability. **A,** Diagram of *in vitro* photothermal therapy and evaluation of cell viability. A total of $1 \times 10^4$ cells were seeded onto 96-well plates. The next day, cells were incubated with sCA alone, free ICG or sCA-ICG for 3 hours. The ICG concentration used for HCT116 and HT29 cells was 20 and 10 μg/mL, respectively. The plate was then placed on the digital water bath to maintain a temperature of 37°C and the cells irradiated using an 808-nm laser with an energy density of 1 W/cm$^2$ for 1, 3, or 5 minutes. After 24 hours, the MTT assay was performed to quantify cell viability. **B,** The cell viability of HCT 116 cells treated with sCA-ICG plus NIR laser irradiation for 1, 3, and 5 minutes was 77.0%, 62.3%, and 42.8 %, respectively, whereas the viability of non-treated cells with irradiation for the indicated times was 86.6%, 96.4%, and 91.3%, sCA plus irradiation; 97.1%, 99.4%, and 97.4%, and ICG plus irradiation; 93.2%, 89.8%, and 76.9%, respectively. **C,** The cell viability of HT29 cells treated with sCA-ICG plus NIR laser irradiation for 1, 3, and 5 minutes was 70.8%, 61.5%, and 58.0%, respectively, whereas the viability of non-treated cells with irradiation for the indicated times was 99.1%, 96.8%, and 99.7%, sCA plus irradiation; 86.5%, 87.1%, and 102.6%, and ICG plus irradiation; 80.8%, 73.3%, and 74.3%. Treatment with sCA plus irradiation showed no significant difference in cell viability when compared with no treatment with irradiation in both cell lines at all time points. In both cell lines, sCA-ICG plus irradiation resulted in significantly lower cell viability than free ICG plus irradiation or sCA plus irradiation at 5 minutes; **, $P < 0.01$. **D** and **E,** The ROS fluorescence image of HCT116 or HT29 cells treated with ICG or sCA-ICG followed by 5 minutes of NIR laser irradiation. A total of $4 \times 10^5$ cells/well were seeded onto 6-well cell culture plates and incubated overnight. The culture medium was changed to medium containing free ICG or sCA-ICG. Three hours later, the cells were incubated with APF for 30 minutes at 37°C. Subsequently, the cells were irradiated with the 808-nm laser at 1 W/cm$^2$ for 5 minutes. ROS fluorescence signals were immediately observed by fluorescence microscopy with excitation at 470 nm and emission at 520 nm; scale bar, 50 μm. **F** and **G,** Mean fluorescence intensity of ROS generation by HCT116 or HT29 cells treated with ICG or sCA-ICG plus 5 minutes of NIR laser irradiation. Intracellular ROS generation was quantified by flow cytometry. Without irradiation, ROS intensities were basal levels (dotted lines); **, $P < 0.01$.

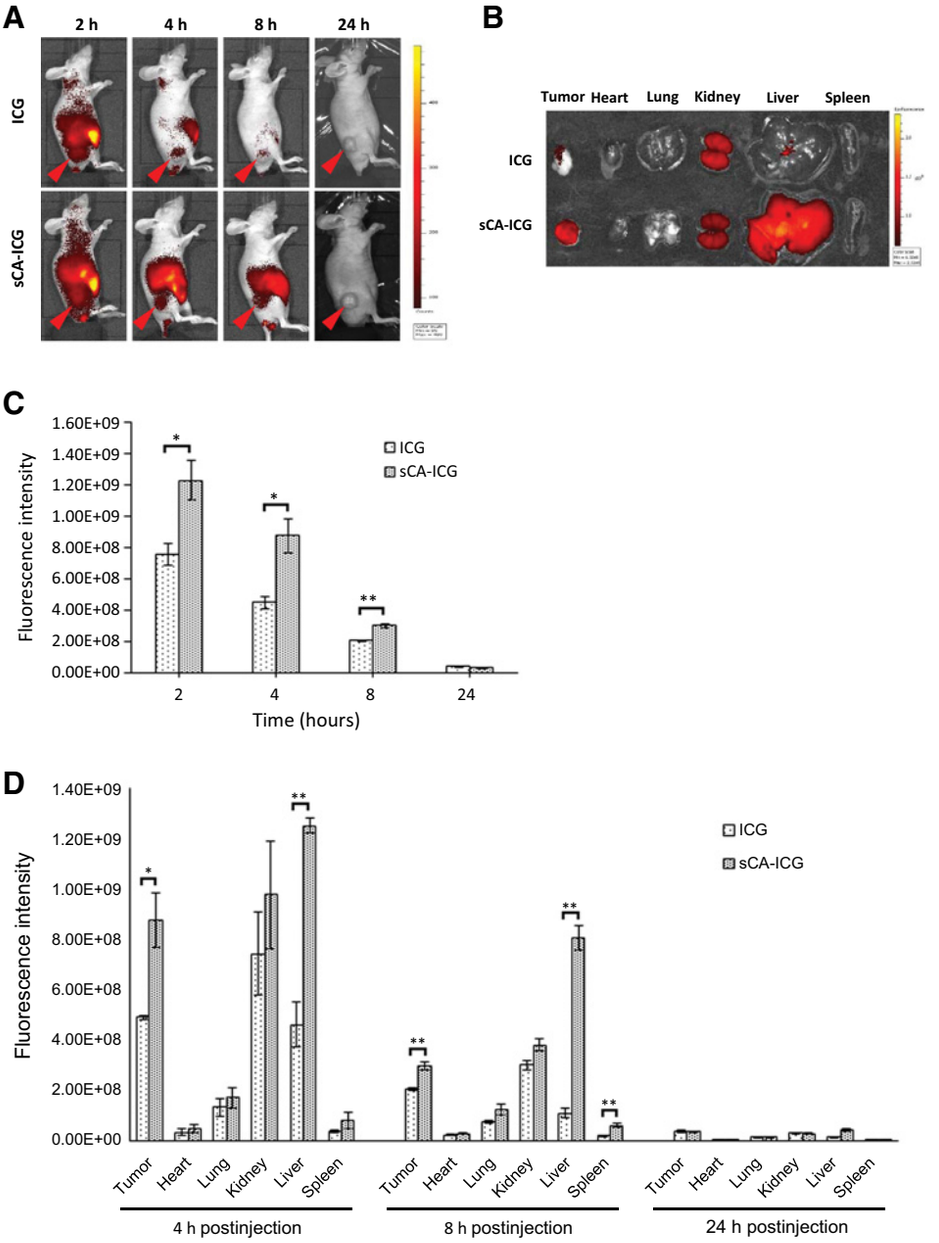


**Figure 5.**

*In vivo* and *ex vivo* fluorescence images of ICG in nude mice harboring HT29 xenografts. **A,** Mice were imaged by IVIS 2, 4, 8, and 24 hours after intravenous dosing with ICG or sCA-ICG (5 mg/kg ICG). **B,** *Ex vivo* images of tumor and major organs 4 hours after injection of free ICG or sCA-ICG. **C,** *Ex vivo* fluorescence intensity of tumors quantified at the indicated time points ($n = 3$ for each group). **D,** Quantitative biodistribution of free ICG or sCA-ICG 4, 8, and 24 hours post-injection ($n = 3$ for each group); *, $P < 0.05$ and **, $P < 0.01$.

of albumin. Furthermore, sCA facilitated cellular uptake of ICG as determined by immunocytochemistry and FACS analysis. Taken together, these results suggest that sCA-ICG is a novel class of PDT through enhanced production of heat and ROS.

In contrast with the progressive increase in ICG uptake to tumor cells *in vitro*, the *in vivo* ICG uptake to tumor xenografts peaked 2 hours after injection and subsequently decreased, with the fluorescence almost gone at 24 hours. In addition to tumors, ICG was distributed predominantly in the liver and kidney at 4 hours and almost disappeared by 24 hours. This quick clearance is based on the *in vivo* metabolism of ICG, which binds to albumin and lipoprotein and is immediately taken up by the liver and excreted from the intestine (43). On the other hand, the situation differed when we also performed a biodistribution study using the commercially available liposome-ICG (GLYCOLIPO, Katayamakagaku, Osaka Japan). Thus, at 24 hours the majority of ICG remained in the tumor and normal organs after injection of liposome-ICG (Supplementary Fig. S3). The fluorescence intensity of ICG remaining in the tumor at 24 hours was almost equal to the intensity 4 hours post-injection. In the kidney and liver, high fluorescence intensities were still observed 24 hours post-injection. These findings emphasize that rapid clearance is a unique characteristic of sCA-ICG and contrasts with other nanoparticle systems, including liposome, doxorubicin, and ICG loaded poly lactic-co-glycolic acid lecithin-polyethylene glycol core-shell nanoparticles (DINP), and CS-AuNR-ICG, which remains a long time in tumors and normal organs due to the acquired stability (21–23, 35–37). Although free ICG has been considered a harmless drug, we are aware of recent studies on the risk of ICG. An *in vitro* study showed that human retinal pigment epithelial cells

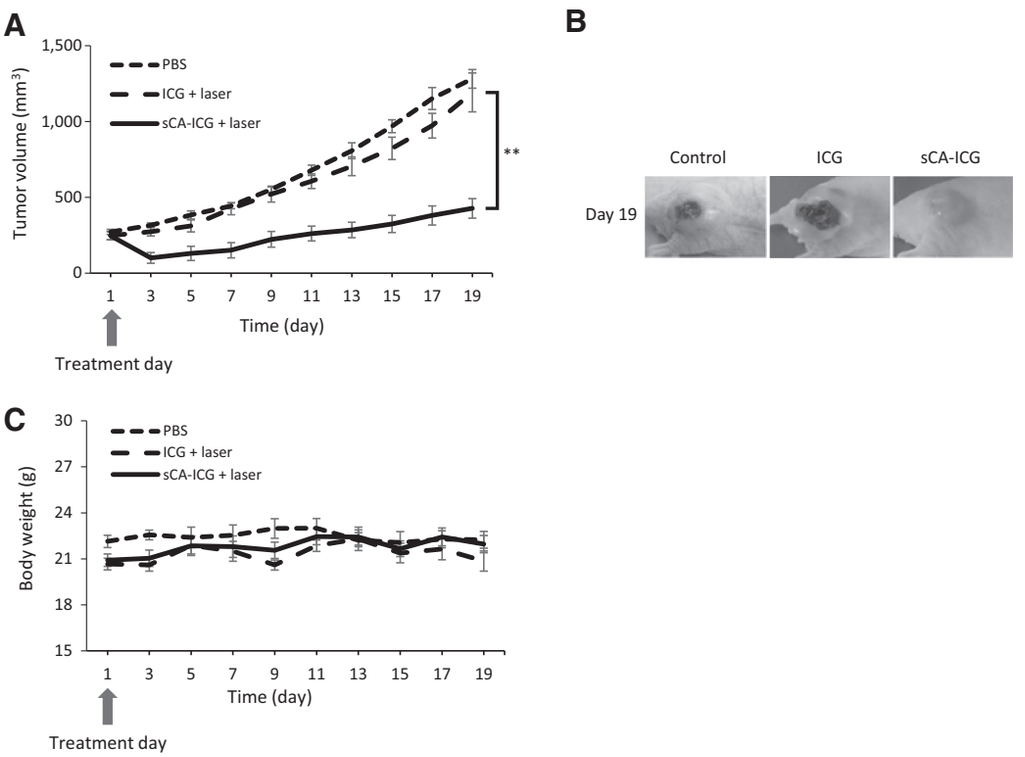


**Figure 6.**

*In vivo* photothermal therapy. **A,** HT29 tumor growth curves for different treatment groups. At a tumor volume of 200 to 300 $mm^3$, mice were randomized into three treatment groups: PBS alone, ICG plus laser, and sCA-ICG plus laser. Mice were administered 200 μL of PBS, free ICG, or sCA-ICG (100 μg ICG per mouse). The tumor region was irradiated with an 808-nm laser for 5 minutes at a power density of 3.7 $W/cm^2$ 4 hours post-injection ($n = 7$ for each group); **, $P < 0.01$. **B,** Representative photographs of tumors on day 19 after treatment. **C,** Body weight of mice after treatment.

produce significant toxicity within 24 hours of exposure to ICG (44). It has also been reported that visual field defects and retinal pigment epithelial atrophy occur when ICG is used to stain the internal limiting membrane of the retina during vitrectomy (45–46). In this regard, rapid exclusion of sCA-ICG from the body may be the ideal nanoplatform to avoid unknown adverse events caused by ICG remaining in the body. In addition, we confirmed that repeat administration of sCA did not cause hepatotoxicity or other severe adverse events in mice (Supplementary Fig. S2).

For *in vivo* PDT experiments, we performed NIR irradiation at 4 hours, when the tumor outline became clear on IVIS. At this time point, the tumor fluorescence in sCA-ICG–treated mice was 2-times higher than that of ICG-treated mice. This ratio was compatible with that employed in previous studies; liposome-ICG at 4 hours post-injection and DINPs at 6 hours post-injection (21, 36). We prepared a challenging condition for tumor therapy. First, we produced relatively large tumors (200–300 $mm^3$), whereas most PDT studies have treated 50–150 $mm^3$ tumors (21, 23, 36–37). For this purpose, we used HT29 cells because they produced solid and homogenous large tumors, though HCT116 tumors readily created central necrosis during tumor growth. Moreover, the dose of ICG used in this study (5 mg/kg) was within the dose range (2–25 mg/kg) used for the PDT studies (21–22, 26, 35–36) and much lower than the maximum dose ($LD_{50}$) of 50–80 mg/kg (47). Despite the rigorous conditions, only one shot of the NIR beam conferred considerable damage to tumors after injection of sCA-ICG and caused considerable tumor inhibition on day 19. In Fig. 6, it appears that only one laser shot given 4 hours after injection of sCA-ICG instantly caused massive tumor death so that the tumor volume rapidly decreased to 34.1% by day 3. Then the remaining tumor cells started to regrow, and gradually recovered its volume to the initial level around day 13. This rather strong effect is one of the characteristics of photodynamic therapy, as the studies have demonstrated it with one shot (11, 12, 22–24, 26, 35, 37, 42, 48). The results also suggest that repeat irradiation may eradicate tumors completely. Because it is reported that talaporfin (excitation light: 664nm) can treat a tumor whose diameter >1.0 cm or more (49–50), more diseases can be candidates for the application of PDT using sCA-ICG plus NIR irradiation considering the deeper reach of NIR. These include invasive carcinoma of the esophagus, cervix, or lung; lymph node metastasis; and tumors on the body surface, including carcinomas of the head and neck, breast and malignant lymphoma, and melanoma.

To further enhance the therapeutic effect of PDT with a single conventional agent, attention has been drawn to dual therapy combining another photosensitizer or anticancer agent (36, 37, 48). Combining drugs with different mechanisms is expected to have synergistic antitumor effects and reduce side effects. We tried to add glucose to ICG in sCA

because we previously reported that the sCA-glucose complex had antitumor effects *in vitro* and *in vivo*, partially due to upregulation of ROS activity (48). Although the additional glucose effects on sCA-ICG were only modest in an *in vitro* PDT study (Supplementary Fig. S4), this result is encouraging because the preliminary data suggest that sCA-ICG should have the potential for dual therapy. As sCA exhibits the best affinity for nucleic acids (29, 31–34), it is likely that sCA-ICG combined with certain molecular targeting may further enhance the effects of PDT. Studies of multidisciplinary PDT are currently underway in our laboratory using sCA-ICG plus siRNA targeting the stress gene *NRF2* or immune checkpoint molecules PD-L1/PD-1.

In conclusion, this study shows that sCA is a useful vehicle for ICG-based PDT. Potent tumor inhibition by PDT and the quick withdrawal of ICG from normal organs was demonstrated, with the latter finding being unique to sCA-ICG and different from the other nanoparticles with high *in vivo* stability. Further investigation using sCA-ICG as a novel platform for PDT in many types of tumors, as well as of the potential possibility of dual therapy, is essential.

## Disclosure of Potential Conflicts of Interest

No potential conflicts of interest were disclosed.

## Authors' Contributions

**Conception and design:** K. Tamai, A. Inoue, J. Nishimura, T. Hata, M. Mori, H. Yamamoto
**Development of methodology:** K. Tamai, X. Wu, A. Inoue, T. Hata, H. Yamamoto
**Acquisition of data (provided animals, acquired and managed patients, provided facilities, etc.):** K. Tamai, A. Inoue, M. Ota, N. Haraguchi, M. Mori
**Analysis and interpretation of data (e.g., statistical analysis, biostatistics, computational analysis):** K. Tamai, A. Inoue, H. Takahashi, M. Mori, H. Yamamoto
**Writing, review, and/or revision of the manuscript:** K. Tamai, T. Mizushima, Y. Yokoyama, N. Haraguchi, T. Hata, M. Mori, H. Yamamoto
**Administrative, technical, or material support (i.e., reporting or organizing data, constructing databases):** K. Tamai, N. Miyoshi
**Study supervision:** A. Inoue, H. Takahashi, J. Nishimura, C. Matsuda, Y. Doki, M. Mori, H. Yamamoto

## Acknowledgments

This work was supported by a grant from JSPS KAKENHI (Grant Number JP 16K18451; to K. Tamai). We are grateful to Keiichiro Yamada for his technical assistance of laser beam apparatus. We express our respect to Emeritus Prof. Toshihiro Akaike (FAIS, Ibaraki, Japan) for developing the original carbonate apatite gene delivery system.

The costs of publication of this article were defrayed in part by the payment of page charges. This article must therefore be hereby marked *advertisement* in accordance with 18 U.S.C. Section 1734 solely to indicate this fact.

Received August 16, 2017; revised December 26, 2017; accepted April 6, 2018; published first April 13, 2018.

## References

1. Allison RR, Mota HC, Bagnato VS, Sibata CH. Bio-nanotechnology and photodynamic therapy-State of the art review. Photodiagnosis Photodyn Ther 2008;5:19–28.
2. Dolmans DE, Fukumura D, Jain RK. Photodynamic therapy for cancer. Nat Rev Cancer 2003;3:380–7.
3. van Straten D, Mashayekhi V, de Bruijn H, Oliveira S, Robinson D. Oncologic photodynamic therapy: basic principles, current clinical status and future directions. Cancers 2017;9:19.
4. Colvin H, Mizushima T, Eguchi H, Takiguchi S, Doki Y, Mori M. Gastroenterological surgery in Japan: The past, the present and the future. Ann Gastroenterol Surg 2017;1:5–10.
5. Kahaleh M, Mishra R, Shami VM, Northup PG, Berg CL, Bashlor P, et al. Unresectable cholangiocarcinoma: comparison of survival in biliary stenting alone versus stenting with photodynamic therapy. Clin Gastroenterol Hepatol 2008;6:290–7.
6. Yano T, Muto M, Minashi K, Iwasaki J, Kojima T, Fuse N, et al. Photodynamic therapy as salvage treatment for local failure after chemoradiotherapy in patients with esophageal squamous cell carcinoma: a phase II study. Int J Cancer 2012;131:1228–34.
7. Rieken M, Bachmann A. Laser treatment of benign prostate enlargement–which laser for which prostate? Nat Rev Urol 2014;11:142–52.
8. Te AE. The next generation in laser treatments and the role of the greenlight high-performance system laser. Rev Urol 2006;8:S24–30.
9. Honda N, Kariyama Y, Hazama H, Ishii T, Kitajima Y, Inoue K, et al. Optical properties of tumor tissues grown on the chorioallantoic membrane of chicken eggs: tumor model to assay of tumor response to photodynamic therapy. J Biomed Opt 2015;20:125001.
10. Chen CW, Chan YC, Hsiao M, Liu RS. Plasmon-enhanced photodynamic cancer therapy by upconversion nanoparticles conjugated with Au Nanorods. ACS Appl Mater Interfaces 2016;8:32108–19.
11. He F, Feng L, Yang P, Liu B, Gai S, Yang G, et al. Enhanced up/down-conversion luminescence and heat: Simultaneously achieving in one single core-shell structure for multimodal imaging guided therapy. Biomaterials 2016;105:77–88.
12. Mitsunaga M, Ogawa M, Kosaka N, Rosenblum LT, Choyke PL, Kobayashi H. Cancer cell–selective in vivo near infrared photoimmunotherapy targeting specific membrane molecules. Nat Med 2011;17:1685–91.
13. Kuriyama M, Yano A, Yoshida Y, Kubo M, Akita S, Mitsukawa N, et al. Reconstruction using a divided latissimus dorsi muscle flap after conventional posterolateral thoracotomy and the effectiveness of indocyanine green-fluorescence angiography to assess intraoperative blood flow. Surg Today 2016;46:326–34.
14. Coufal O, Fait V. Use of indocyanine green and the HyperEye system for detecting sentinel lymph nodes in breast cancer within a population of European patients: a pilot study. World J Surg Oncol 2016;14:299.
15. Lau L, Christophi C, Muralidharan V. Intraoperative functional liver remnant assessment with indocyanine green clearance: another toehold for climbing the "ALPPS." Ann Surg 2015;261:e43–5.
16. Nomori H, Cong Y, Sugimura H. Utility and pitfalls of sentinel node identification using indocyanine green during segmentectomy for cT1N0M0 non-small cell lung cancer. Surg Today 2016;46:908–13.
17. Radzi R, Osaki T, Tsuka T, Imagawa T, Minami S, Okamoto Y. Morphological study in B16F10 murine melanoma cells after photodynamic hyperthermal therapy with indocyanine green (ICG). J Vet Med Sci 2012;74:465–72.
18. Luo S, Zhang E, Su Y, Cheng T, Shi C. A review of NIR dyes in cancer targeting and imaging. Biomaterials 2011;32:7127–38.
19. Yoneya S, Saito T, Komatsu Y, Koyama I, Takahashi K, Duvoll-Young J. Binding properties of indocyanine green in human blood. Invest Ophthalmol Vis Sci 1998;39:1286–90.
20. Urbanska K, Romanowska-Dixon B, Matuszak Z, Oszajca J, Nowak-Sliwinska P, Stochel G. Indocyanine green as a prospective sensitizer for photodynamic therapy of melanomas. Acta Biochim Pol 2002;49:387–91.
21. Shemesh CS, Moshkelani D, Zhang H. Thermosensitive liposome formulated indocyanine green for near-infrared triggered photodynamic therapy: in vivo evaluation for triple-negative breast cancer. Pharm Res 2015;32:1604–14.
22. Zheng M, Zhao P, Luo Z, Gong P, Zheng C, Zhang P, et al. Robust ICG theranostic nanoparticles for folate targeted cancer imaging and highly effective photothermal therapy. ACS Appl Mater Interfaces 2014;6:6709–16.
23. Sheng Z, Hu D, Zheng M, Zhao P, Liu H, Gao D, et al. Smart human serum almubin-indocyanine green nanoparticles generated by programmed assembly for dual-modal imaging guided cancer synergistic phototherapy. ACS Nano 2014;12310–22.

24. Huang P, Gao Y, Lin J, Hu H, Liao H, Yan X, et al. Tumor-Specific formation of enzyme-instructed supramolecular self-assemblies as cancer theranostics. ACS Nano 2015;9:9517–27.
25. Tsujimoto H, Morimoto Y, Takahata R, Nomura S, Yoshida K, Horiguchi H, et al. Photodynamic therapy using nanoparticle loaded with indocyanine green for experimental peritoneal dissemination of gastric cancer. Cancer Sci 2014;105:1626–30.
26. Zheng X, Zhou F, Wu B, Chen WR, Xing D. Enhanced tumor treatment using biofunctional indocyanine green-containing nanostructure by intratumoral or intravenous injection. Mol Pharm 2012;9:514–22.
27. Kobayashi H, Watanabe R, Choyke PL. Improving conventional enhanced permeability and retention (EPR) effects; what is the appropriate target? Theranostics 2014;4:81–9.
28. Chua MJ, Tiash S, Fatemian T, Noordin MI, Keng CS, Chowdhury EH. Carbonate apatite-facilitated intracellular delivery of c-ROS1 small interfering RNA sensitises MCF-7 breast cancer cells to cisplatin and paclitaxel. OA Cancer 2013;1:7.
29. Wu X, Yamamoto H, Nakanishi H, Yamamoto Y, Inoue A, Tei M, et al. Innovative delivery of siRNA to solid tumors by super carbonate apatite. PLoS One 2015;10:e0116022.
30. Hossain S, Yamamoto H, Chowdhury EH, Wu X, Hirose H, Haque A, et al. Fabrication and intracellular delivery of doxorubicin/carbonate apatite nanocomposites: effect on growth retardation of established colon tumor. PLoS ONE 2013;8:e60428.
31. Hiraki M, Nishimura J, Takahashi H, Wu X, Takahashi Y, Miyo M, et al. Concurrent targeting of KRAS and AKT by MiR-4689 is a novel treatment against mutant KRAS colorectal cancer. Mol Ther Nucleic Acids 2015;4:e231.
32. Takahashi H, Nishimura J, Kagawa Y, Kano Y, Takahashi Y, Wu X, et al. Significance of polypyrimidine tract-binding protein 1 expression in colorectal cancer. Mol Cancer Ther 2015;14:1705–16.
33. Takeyama H, Yamamoto H, Yamashita S, Wu X, Takahashi H, Nishimura J, et al. Decreased miR-340 expression in bone marrow is associated with liver metastasis of colorectal cancer. Mol Cancer Ther 2014;13:976–85.
34. Ogawa H, Wu X, Kawamoto K, Nishida N, Konno M, Koseki J, et al. MicroRNAs induce epigenetic reprogramming and suppress malignant phenotypes of human colon cancer cells. PLoS 2015;10:e0127119.
35. Maruyama T, Akutsu Y, Suganami A, Tamura Y, Fujito H, Ouchi T, et al. Treatment of near-infrared photodynamic therapy using a liposomally formulated indocyanine green derivative for squamous cell carcinoma. PLoS ONE 2015;10:e0122849.
36. Zheng M, Yue C, Ma Y, Gong P, Zhao P, Zheng C, et al. Single-step assembly of DOX/ICG loaded lipid – polymer nanoparticles for highly effective chemo-photothermal combination therapy. ACS Nano 2013;7:2056–67.
37. Chen R, Wang X, Yao X, Zheng X, Wang J, Jiang X. Near-IR-triggered photothermal/photodynamic dual-modality therapy system via chitosan hybrid nanospheres. Biomaterials 2013;34:8314–22.
38. Perrault SD, Walkey C, Jennings T, Fischer HC, Chan WC. Mediating tumor targeting efficiency of nanoparticles through design. Nano Lett 2009;9:1909–15.
39. Cabral H, Matsumoto Y, Mizuno K, Chen Q, Murakami M, Kimura M, et al. Accumulation of sub-100 nm polymeric micelles in poorly permeable tumours depends on size. Nat Nanotechnol 2011;6:815–23.
40. Chowdhury EH, Akaike T. A bio-recognition device developed onto nanocrystals of carbonate apatite for cell-targeted gene delivery. Biotechnol Bioeng 2005;90:414–21.
41. Chen S, Yu G, Zhang B, Wang Y, Zhang N, Chen Y. Human serum albumin (HSA) coated liposomal indocyanine green for in vivo tumor imaging. RSC Adv 2016; 6:15220–5.
42. Cui S, Yin D, Chen Y, Di Y, Chen H, Ma Y, et al. In vivo targeted deep-tissue photodynamic therapy based on near-infrared light triggered upconversion nanoconstruct. ACS Nano 2013;7:676–88.
43. Onda N, Kimura M, Yoshida T, Shibutani M. Preferential tumor cellular uptake and retention of indocyanine green for in vivo tumor imaging. Int J Cancer 2016;139:673–82.
44. Morales MC, Freire V, Asumendi A, Araiz J, Herrera I, Castiella G, et al. Comparative effects of six intraocular vital dyes on retinal pigment epithelial cell. Investig Ophthalmol Vis Sci 2010;51:6018–29.
45. Ikagawa H, Yoneda M, Iwaki M, Isogai Z, Tsujii K, Yamazaki R, et al. Chemical toxicity of indocyanine green damages retinal pigment epithelium. Invest Ophthalmol Vis Sci 2005;46:2531–9.
46. Iriyama A, Uchida S, Yanagi Y, Tamaki Y, Inoue Y, Matsuura K, et al. Effects of indocyanine green on retinal ganglion cells. Invest Ophthalmol 2004; 45:943–7.
47. Taichman GC, Hendry PJ, Keon WJ. The use of cardio-green for intraoperative visualization of the coronary circulation: evaluation of myocardial toxicity. Tex Heart Inst J 1987;14:133–8.
48. Yamamoto H, Wu X, Nakanishi H, Yamamoto Y, Uemura M, Hata T, et al. A glucose carbonate apatite complex exhibits *in vitro* and *in vivo* anti-tumour effects. Sci Rep 2015;5:7742.
49. Usuda J, Ichinose S, Ishizumi T, Hayashi H, Ohtani K, Maehara S, et al. Outcome of photodynamic therapy using NPe6 for bronchogenic carcinomas in central airways >1.0 cm in diameter. Clin Cancer Res 2010; 16:2198–204.
50. Muragaki Y, Akimoto J, Maruyama T, Iseki H, Ikuta S, Nitta M, et al. Phase II clinical study on intraoperative photodynamic therapy with talaporfin sodium and semiconductor laser in patients with malignant brain tumors. J Neurosurg 2013;119:845–52.